Supporting Information

Refining active sites and hydrogen spillover for boosting visible-light-driven ammonia synthesis at room temperature

Rong Fu,[‡a] Ziye Pan,[‡a] Xiaowei Mu,[a] Jiayang Li,[a] Qingyun Zhan,[a] Zihan Zhao,[a] Xiaoyue Mu[b] and Lu Li* [a,b]

*Corresponding author. Email: luli@jlu.edu.cn

Materials and Methods

1. Materials.

Titanium tetrachloride ($TiCl_4$), Chloroplatinic acid hexahydrate, Molybdenum acetylacetonate and Tetrahydrofuran (THF) were purchased from Aladdin. Anhydrous ethanol (AR grade) and acetone (CP grade) were purchased from Sinopharm Chemical Reagent Co, Ltd. All chemicals were used without further purification. The purities of hydrogen, nitrogen and argon are all 99.995%. To eliminate any possible NH_3 and NO_x impurities in the N_2 feed gas, the N_2 feed gas was purified by using H_2SO_4 and H_2O as the adsorbent.

2. Preparation of TiO_{2-x}.

TiO_{2-x} was prepared by the solvothermal method using titanium tetrachloride ($TiCl_4$) as precursors. Specifically, 2 mL (3.46 g) of $TiCl_4$ (99%) was added dropwise into 50 mL of ethanol and then transferred into the Teflon-lined stainless steel autoclave, followed by heating at 453 K for 24 h under the autogenous pressure. The resulting solid product was recovered by centrifugation, washed with anhydrous ethanol and distilled water several times and dried at room temperature in a vacuum drying oven. The BET surface area of the as-synthesized TiO_{2-x} was measured to be 124.1 m^2/g.

3. Preparation of Mo-TiO_{2-x}.

Mo-TiO_{2-x} was prepared by the solvothermal method using titanium tetrachloride ($TiCl_4$) and molybdenum acetylacetonate as precursors. Specifically, 58 mg of $C_{10}H_{14}MoO_6$ powder was dissolved into 50 mL of ethanol. The suspension was vigorously stirred for 30 minutes at room temperature to prepare a yellow transparent solution. Then, 2 mL of $TiCl_4$ was added into the above solution drop by drop. The molar ratio of Mo and Ti is 1:100. The finally obtained yellow transparent solution was transferred into the autoclave, which was heated at 453 K for 24 h under the autogenous pressure and then naturally cooled to room temperature. The resultant product was separated by centrifugation and washed with anhydrous ethanol and distilled water several times. The corresponding products were dried at room temperature in a vacuum drying oven. Following the same procedure, a series of Mo-TiO_{2-x} with different Mo content can be prepared by simply changing the amount of $C_{10}H_{14}MoO_6$ added. The BET surface areas of Mo-TiO_{2-x} with different Mo content are listed below.

Mo:Ti (at%)	S_{BET} (m^2/g)
0.5	125.9
1	129.2
5	132.6
10	142.6
20	144.8

4. Preparation of Pt@Mo-TiO_{2-x}.

Platinum loading was conducted via the photoreduction of the as-synthesized Mo-TiO_{2-x} with $H_2PtCl_6 \cdot 6H_2O$. Firstly, 0.1 g of Mo-TiO_{2-x} was ultrasonically dispersed in a mixture of 40 mL methanol and 10 mL deionized water. 2.66 mg of $H_2PtCl_6 \cdot 6H_2O$ was added into the above mixture and stirred for 2 h in the dark under vacuum. Afterward, the solution was irradiated under a 300-W xenon lamp for 30 min. The resulting solid product was recovered by centrifugation, washed with anhydrous ethanol and distilled water several times and dried at room temperature in a vacuum drying oven. The finally obtained sample was designated as Pt@Mo-TiO_{2-x}, Pt content: 1.0 wt%. Following the same procedure, a series of Pt@Mo-TiO_{2-x} with different Pt content can be prepared by simply changing the amount of $H_2PtCl_6 \cdot 6H_2O$ added.

5. Density functional theory (DFT) calculations

All the Density Functional Theory (DFT) calculations [1, 2] were performed in Vienna Ab Initio Simulation Package (VASP) [3, 4]. The exchange-correlation functional was modeled by the generalized gradient approximation (GGA) with the Perdew-Burke-Ernzerhof (PBE) realization [5]. The interaction between the ionic core and the valence electrons was described by the projector-augmented wave (PAW) method [6, 7] , For structural relaxation, the convergence criteria for energy and force were 10^{-4} eV and 0.01 eV·$Å^{-1}$. A (2 × 2 × 2) anatase supercell, with 96 atoms, was constructed using the computed lattice parameters given above for undoped anatase and Mo was substitutionally doped at a Ti site to give a dopant concentration of 3.1 at%. One O atom is subtracted to simulate oxygen vacancies. For structural optimization, we sampled 7 × 7 × 3 Gramma k-points in the Brillouin zone.

The anatase TiO_2 bulk was used to construct the periodic slabs for the (101) surface calculations, which contains four Ti_8O_{16} layers. A vacuum layer of ~15 Å thick was added to minimize the artificial interactions between the surface and its periodic images. During the optimization, the bottom two layers were kept fixed, while the top two layers and the adsorbents were fully relaxed. A 2 × 3 × 1 Gramma k-points was used for the (101) slab. The Mo atom replace 5-fold or 6-fold coordinated Ti atoms on the (101) surface of anatase TiO_2, which is named as Mo_{5c} and Mo_{6c}. One O atom is subtracted from the surface of the model to simulate oxygen vacancies. The electronic structure of Ti was treated in with DFT+U method [8, 9] using a U value of 4.2 eV [10]. Bader charge analysis was used to describe charge distributions [11].

The adsorption energies (E_{ad}) of molecule were defined as Equation (1):

$$E_{ad} = E_{total} - E_{surf} - E_{mole} \qquad (1)$$

where E_{total}, E_{surf}, and E_{mole} are the energies of adsorption configurations, slab models, and free gas molecules.

Differential Charge Density (DCD) was adopted to qualitatively evaluate the charge density

difference $\Delta\rho$ (r), which can be defined as Equation (2)

$$\Delta\rho\ (r)= \rho_{ad}\ (r) - \rho_{surf}\ (r) -\rho_{mole}\ (r) \qquad (2)$$

Where ρ_{ad} (r) represents the total charge density of the fully relaxed configuration of N_2 adsorption on Mo-TiO_{2-x} surface. ρ_{surf} (r) and ρ_{mole} (r) are the total electronic charge densities of the separated Mo-TiO_{2-x} surface and N_2, respectively, which maintain the same geometrical structures as in the relaxed N_2 adsorption system. Accordingly, a positive or negative sign $\Delta\rho$ (r) can be used as an indication of whether the charges at that site are increasing or depleting.

6. General characterization

The XRD spectrum of the samples were performed on a Rigaku D/Max 2500/PV X-ray diffractometer with monochromator Cu Kα radiatio（λ=0.15418 nm） from 20° to 70° with the scanning rate of 6°/min. Transmission electron microscope (TEM) were measured using a Tecnai G2 S-Twin F20 with 200 kV accelerating voltage of electron beam. The morphologies and EDX of the obtained power were identified by using field emission scanning electron microscopy (SEM) on a Helios NanoLab 600I from FEI Company. X-ray photoelectron spectroscopy (XPS) was recorded with a Thermo ESCALab 250 annalyzer operating at the constant analyze energy mode and using monochromatic Al Kα radiation. The UV-vis diffuse reflectance spectra were recorded on a Perkin-Elmer Lambda 950 UV-vis spectrometer. $BaSO_4$ was used as a reflectance standard in a UV-VIS diffuse reflectance experiment. Fourier transform infrared (FTIR) spectroscopy was performed on a Bruker VERTEX Analyzer on samples mixed in KBr pellets, the wavenumber ranged from 400 cm^{-1}-4000 cm^{-1}. The photocurrent response was investigated using CHI 660E electrochemical analyzers (Shanghai Chenhua Apparatus, China). All measurements were taken in a standard three-electrode cell system. A Pt slice was used as the counter electrode, and a Hg/HgO electrode was used as the reference electrode in 0.5 M Na_2SO_4. The electron paramagnetic resonance spectra were obtained on a JES-FA 200 EPR spectrometer. The details of the instrumental parameters were as follows: scanning frequency: 9.45 GHz; scanning width: 800 mT; scanning power: 0.998 mW; scanning temperature: 293 K. The

Brunauer-Emmett-Teller (BET) surface areas of the samples were measured from the adsorption of N_2 at 77 K by using a Micromeritics ASAP 2020M system.

7. Quantification of NH_3 by ion chromatography method

Firstly, we need to prepare a series of ammonium chloride standard solutions of different concentrations (0, 50, 100, 200, 300, 400 and 500 μM), and then 1 mL of ammonium chloride standard solution was injected into the ion chromatography. The calibration curve of ammonia was obtained by using different concentrations of ammonium chloride (see below). As for the generated ammonia in the photocatalytic reaction, 2 mL deionized water was injected into the quartz reactor to fully dissolve the ammonia gas in the product and then the rests were the same as the above steps to determine ammonia concentration by the calibration curve.

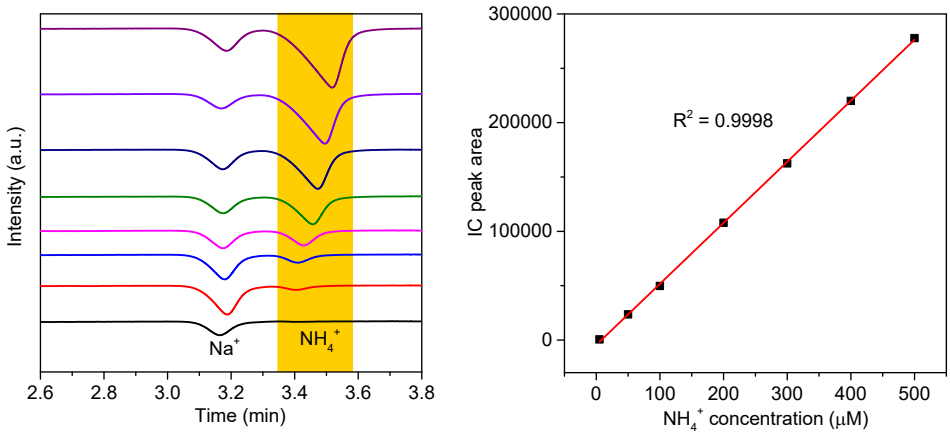

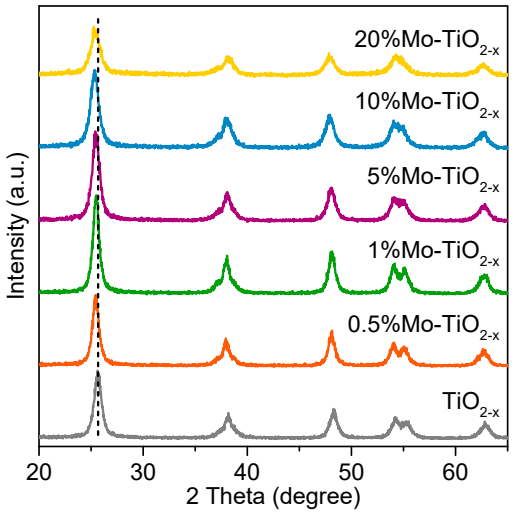

Fig. S1 Powder XRD patterns of TiO_{2-x} and various Mo-TiO_{2-x} samples with different Mo contents.

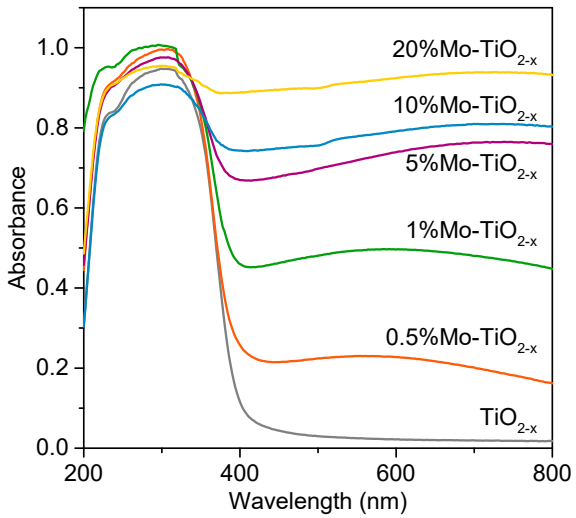

Fig. S2 UV/Vis diffuse reflectance spectra of TiO_{2-x} and various Mo-TiO_{2-x} samples with different Mo contents.

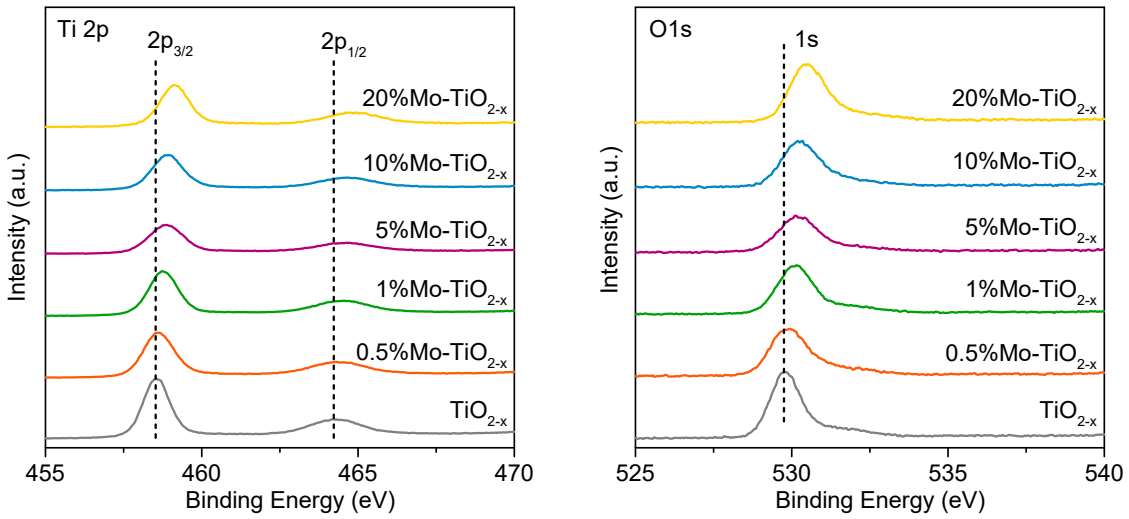

Fig. S3 XPS spectra of Ti 2p (left) and O 1s (right) for TiO_{2-x} and various Mo-TiO_{2-x} samples with different Mo contents.

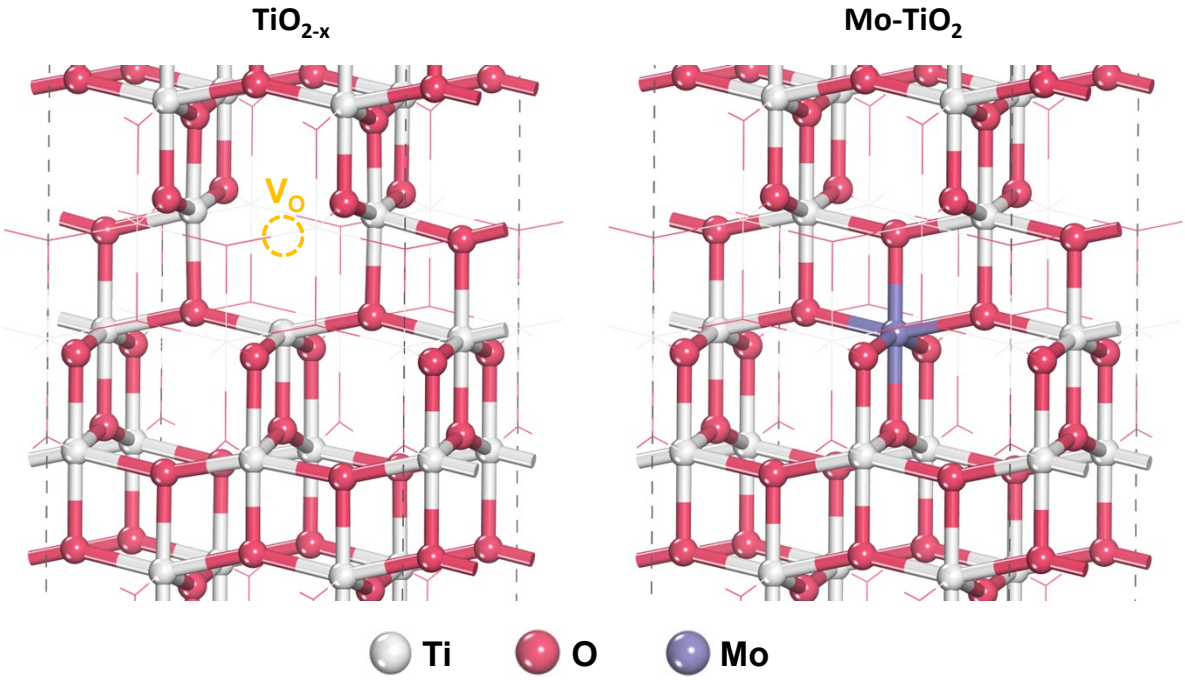

Fig. S4 The optimized structures of TiO_{2-x} (left) and Mo-TiO_2 (right).

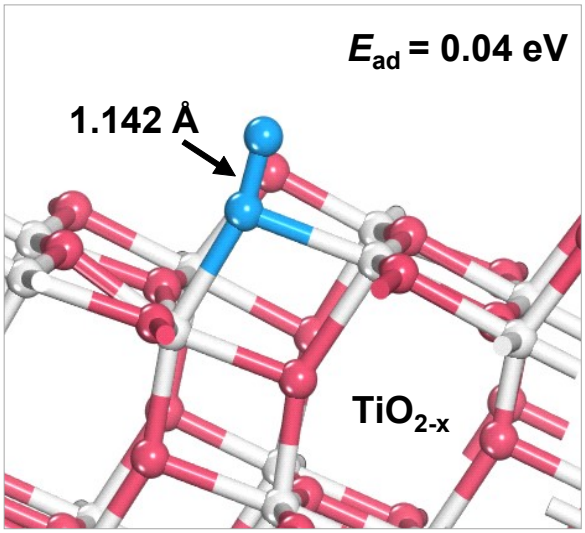

Fig. S5 The optimized configuration of N_2 adsorption on the (101) surface of TiO_{2-x}.

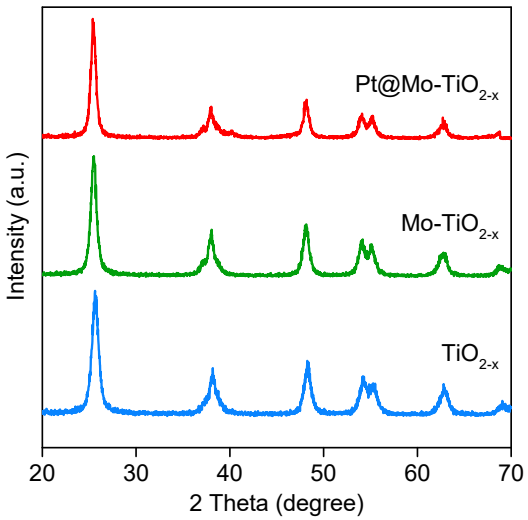

Fig. S6 Powder XRD patterns of TiO_{2-x}, Mo-TiO_{2-x} and Pt@Mo-TiO_{2-x}.

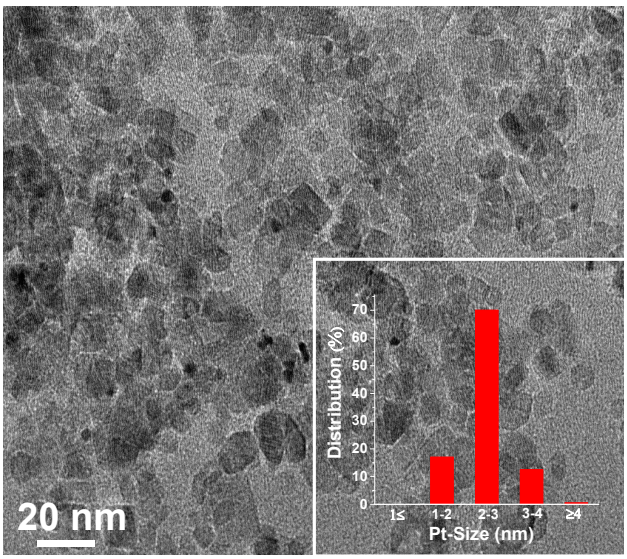

Fig. S7 TEM image of Pt@Mo-TiO_{2-x} (Pt content: 1.0 wt%, Mo:Ti=1:100). The inset histogram shows the diameter distributions of Pt nanoparticles on Pt@Mo-TiO_{2-x}.

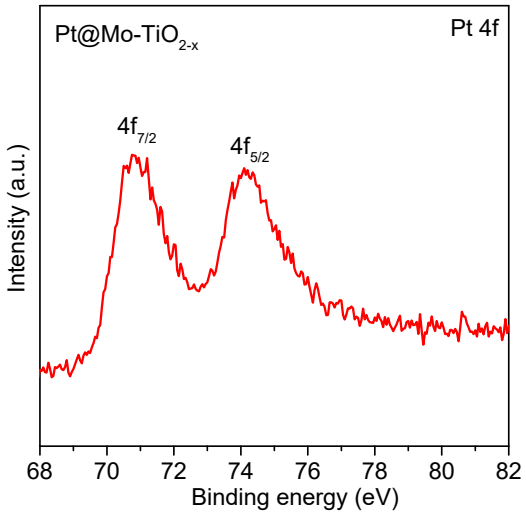

Fig. S8 XPS spectra of Pt 4f for Pt@Mo-TiO_{2-x} (Pt content: 1.0 wt%, Mo:Ti=1:100).

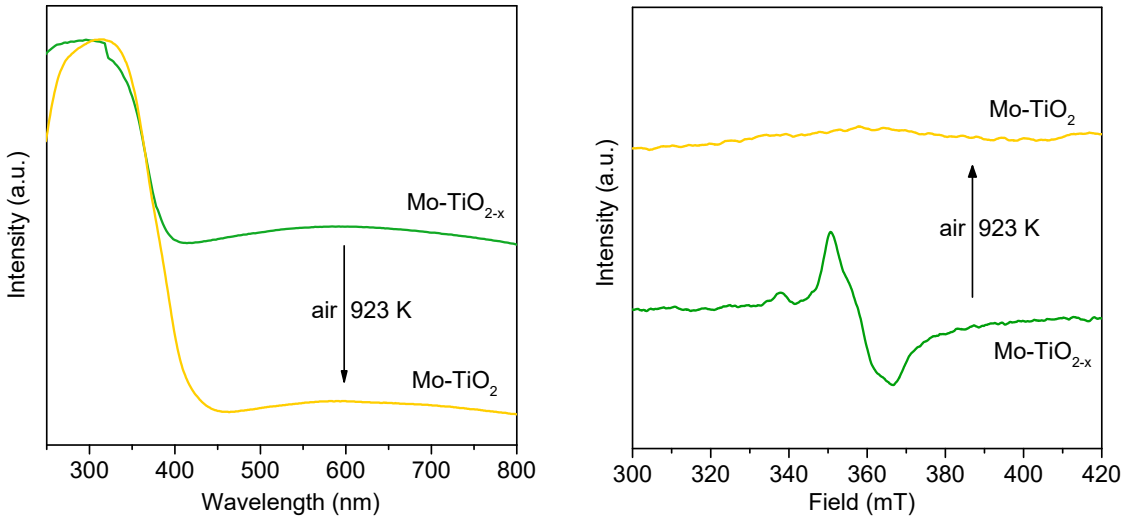

Fig. S9 UV/Vis diffuse reflectance spectra (left) and X-band EPR spectra (right) of Mo-TiO_{2-x} and Mo-TiO_2.

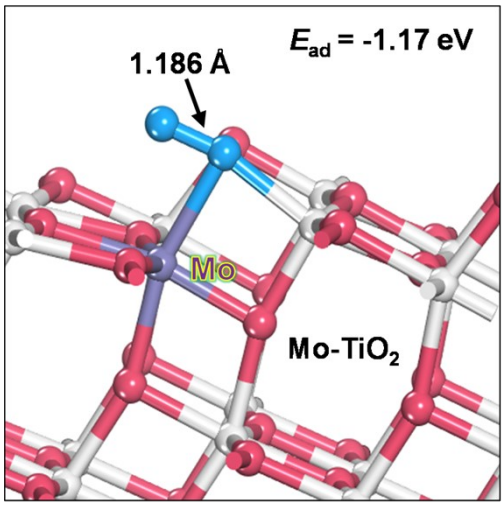

Fig. S10 The optimized configuration of N_2 adsorption on the (101) surface of Mo-TiO_2.

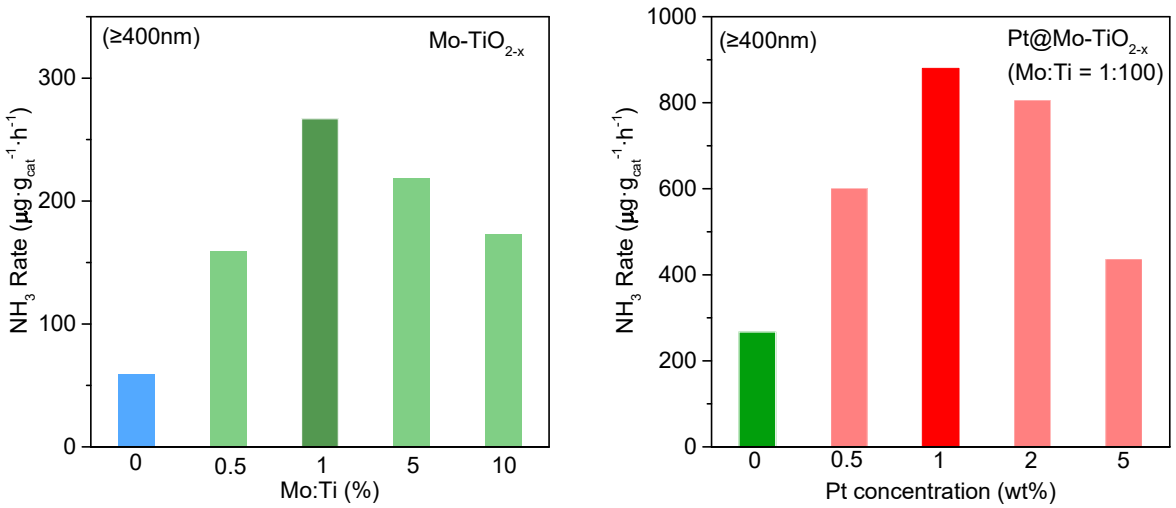

Fig. S11 Ammonia synthesis rate of various Mo-TiO_{2-x} with different Mo doping (left) and various Pt@Mo-TiO_{2-x} with different Pt loading (Mo:Ti=1:100) (right).

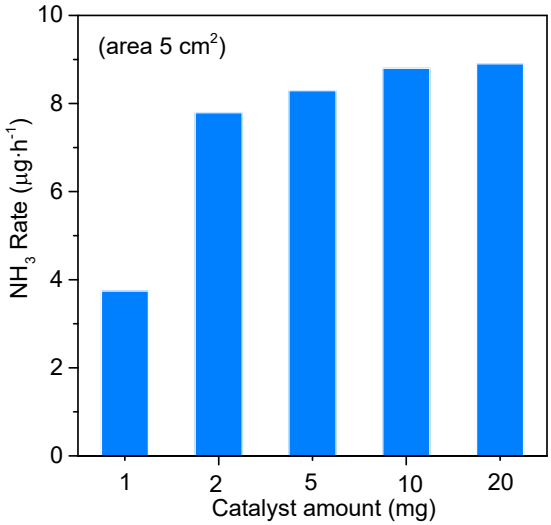

Fig. S12 Ammonia synthesis rate of Pt@Mo-TiO_{2-x} with different catalyst dosages.

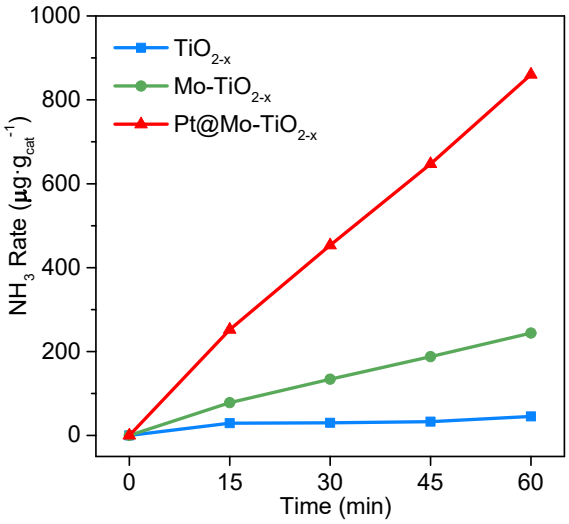

Fig. S13 Photocatalytic ammonia synthesis as a function of time.

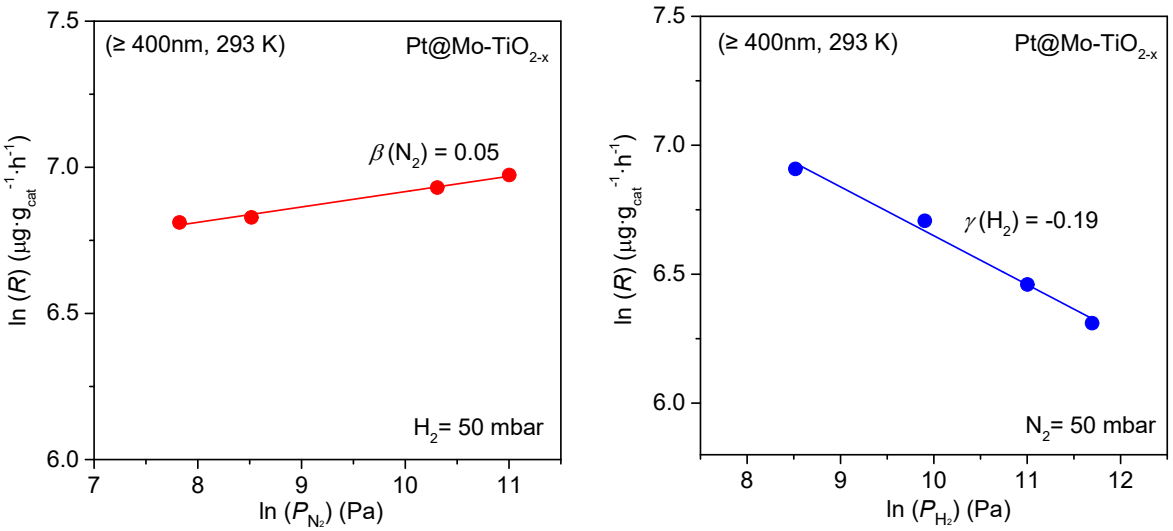

Fig. S14 Dependence of ammonia synthesis rate on the partial pressures of N_2 (left) and H_2 (right) on Pt@Mo-TiO_{2-x} at 293 K.

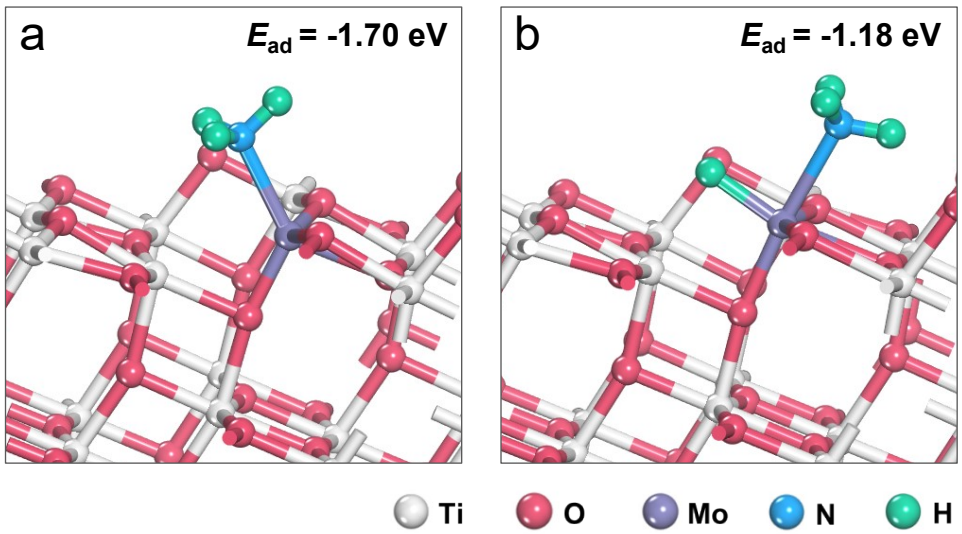

Fig. S15 The optimized configurations of NH_3 adsorption on the (101) surface of (a) Mo-TiO_{2-x} and (b) Mo-TiO_{2-x}-$H_{spillover}$.

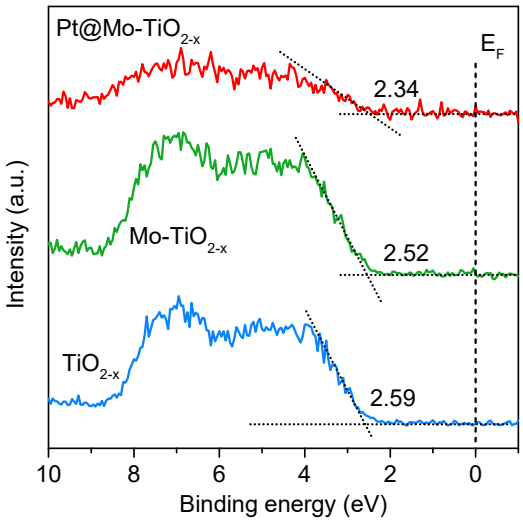

Fig. S16 XPS valence band spectra of TiO_{2-x}, Mo-TiO_{2-x} and Pt@Mo-TiO_{2-x}.

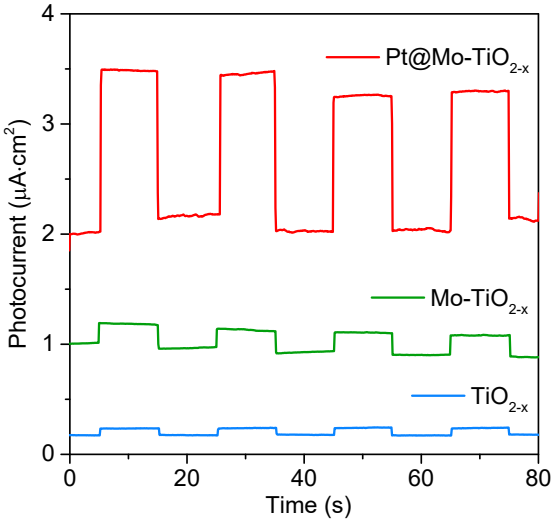

Fig. S17 Photocurrent responses of TiO_{2-x}, Mo-TiO_{2-x} and Pt@Mo-TiO_{2-x}.

Table S1. Representative works on photocatalytic nitrogen fixation.

Entry	Catalysts	Conditions	Reactant	Temperature (K)	NH_3 rate ($\mu g\ g^{-1}\ h^{-1}$)	Ref.
1	TiO_2	Full spectrum	N_2/H_2O	311	18.1	(*12*)
2	Pt-TiO_2	Full spectrum	N_2/H_2O	311	31.7	(*12*)
3	JRC-TIO-6 (rutile)	UV light ($\lambda > 254$ nm)	N_2/H_2O	313	62	(*13*)
4	Cu doped TiO_2	Full spectrum	N_2/H_2O	298	1341.3	(*14*)
5	Fe-doped TiO_2	Full spectrum	N_2/H_2O	313	195.5	(*15*)
6	Defect TiO_2	$\lambda \geq 280$ nm	N_2/H_2O	313	12.41	(*16*)
7	5%Ru@GaN NWs	UV light (290-350 nm)	N_2/H_2	293	2040	(*17*)
8	5%Ru@InGaN NWs	Visible light (400-800 nm)	N_2/H_2	293	46	(*17*)
9	3%FePt@g-C_3N_4	Visible light (400-800 nm)	N_2/H_2	293	63	(*18*)
10	Fe@graphene	UV light ($\lambda < 400$ nm)	N_2/H_2	473	408	(*19*)
11	Fe-Al@graphene	UV light ($\lambda < 400$ nm)	N_2/H_2	473	430.1	(*20*)
12	2%Ru@F-TiO_{2-x}	Visible light (400-1550 nm)	N_2/H_2	293	118.5	(*21*)
13	2%Ru@F-Film	Visible light (400-1550 nm)	N_2/H_2	293	1092	(*21*)
14	Pt@Mo-TiO_{2-x}	Visible light (400-800 nm)	N_2/H_2	293	880	*This work*
15	Pt@Mo-TiO_{2-x}-Film	Visible light (400-800 nm)	N_2/H_2	293	3784	*This work*

Reference

[S1] W. Kohn and L. J. Sham, *Phys. Rev.* 1965, **140**, 1133-1138.

[S2] P. Hohenberg and W. Kohn, *Phys. Rev.* 1964, **136**, 864-871.

[S3] G. Kresse and J. Hafner, *Phys. Rev. B.* 1994, **49**, 14251-14269.

[S4] G. Kresse and J. Furthmüller, *Phys. Rev. B.* 1996, **54**, 11169-11185.

[S5] J. P. Perdew, K. Burke and M. Ernzerhof, *Phys. Rev. Lett.* 1996, **77**, 3865-3868.

[S6] P. E. Blochl, *Phys. Rev. B.* 1994, **50**, 17953-17979.

[S7] G. Kresse and D. Joubert, *Phys. Rev. B.* 1999, **59**, 1758-1775.

[S8] S. L. Dudarev, G. A. Botton, S. Y. Savrasov, C. J. Humphreys and A. P. Sutton, *Phys. Rev. B.* 1998, **57**, 1505-1509.

[S9] V. V. Anisimov, J. Zaanen and O. K. Andersen, *Phys. Rev. B.* 1991, **44** , 943-954.

[S10] M. Nolan, *Chem. Commun.* 2011, **47**, 8617-8619.

[S11] G. Henkelman, A. Arnaldsson and H. Jónsson, *Comput. Mater. Sci.* 2006, **36**, 354-360.

[S12] H. Miyama, N. Fujii and Y. Nagae, *Chem. Phys. Lett.* 1980, **74**, 523-524.

[S13] H. Hirakawa, M. Hashimoto, Y. Shiraishi and T.Hirai, *J. Am. Chem. Soc.* 2017, **139**, 10929-10936.

[S14] Y. Zhao, R. Shi, B. Wang, G. Waterhouse, L. Wu, C. Tung and T. Zhang, *Adv. Mater*. 2019, **31**, 1806482.

[S15] G. Schrauzer and T. Guth, *J. Am. Chem. Soc*. 1977, **99**, 7189

[S16] H. Hirakawa, M. Hashimoto, Y. Shiraishi and T. Hirai, *J. Am. Chem. Soc.* 2017, **139**, 10929-10936.

[S17] L. Li, Y. Wang, S. Vanka, X. Mu, Z. Mi and C.-J. Li, *Angew. Chem. Int. Ed.* 2017, **56***,* 8701-8705.

[S18] Z. Li, Z. Gao, B. Li, L. Zhang, R. Fu, Y. Li, X. Mu and L. Li, *Appl. Catal. B-environ.* 2020, **262***,* 118276.

[S19] Y. Lu, Y. Yang, T. Zhang, Z. Ge, H. Chang, P. Xiao, Y. Xie, L. Hua, Q. Li, H. Li, B. Ma, N. Guan, Y. Ma and Y. Chen, *ACS Nano*. 2016, **10**, 10507-10515.

[S20] Y. Yang, T. Zhang, Z. Ge, Y. Lu and Y. Chen, *Carbon* 2017, **124**, 72-78.

[S21] R. Fu, Z. Wu, Z. Pan, Z. Gao, Z. Li, X. Kong and L. Li, *Angew. Chem. Int. Ed.* 2021, **60**, 11173-11179.